Ab-initio study of the vibrational properties of $Mg(AlH_4)_2$

E. Spanò and M. Bernasconi
Consorzio Corimav, Dipartimento di Scienza dei Materiali and Istituto Nazionale di Fisica per la Materia, Università di Milano-Bicocca, Via Cozzi 53, I-20125, Milano, Italy

Based on Density Functional Theory and Density Functional Perturbation Theory we have studied the thermodynamical and vibrational properties of $Mg(AlH_4)_2$. The crystal structure recently proposed on the basis of x-ray powder diffraction data has been confirmed theoretically by the comparison of the experimental and theoretical IR and Raman spectra. The main discrepancy regards the position of the hydrogen atoms which makes the theoretical AlH_4 tetrahedra more symmetric than the experimental ones. The calculated thermodynamical decomposition temperature is also in good agreement with experimental result.

I. INTRODUCTION

In the search for suitable materials for reversible hydrogen storage the class of metal alanates has attracted much attention in recent years due to their high hydrogen content, but primarly because of the possibility to accelerate the kinetics of hydrogen uptake by doping[1,2]. Sodium alanate, the prototypical material of this class, has long been known. Although its thermodynamics decomposition temperature with hydrogen release is relatively low, the kinetics of the dehydrogenation/rehydrogenation reactions is very slow. The interest in this material for hydrogen storage increased dramatically in 1997 when Bogdanovic *et al.*[1] demonstrated that reversible storage can be achieved at moderate temperature and hydrogen partial pressure by the addition of catalysts, most notably titanium. This discovery boosted an intense activity on the study of other members of the alkali metal alanates as well[3,4].

More recently, magnesium alanate $Mg(AlH_4)_2$, as a representative of the alkali earth metal alanates, has also been considered as a possible materials for hydrogen storage[5,6,7,8]. $Mg(AlH_4)_2$ decomposes readly in the temperature range 110 ^{o}C - 200 ^{o}C according to the reaction

$$Mg(AlH_4)_2 \rightarrow MgH_2 + 2Al + 3H_2 \qquad (1)$$

which would correspond to a maximum reversible hydrogen content of 7 wt%. Although the reversibility of reaction 1 has not been demonstrated yet, the easy of the decomposition reaction even in the absence of doping, suggests that, in analogy with $NaAlH_4$, the insertion of suitable catalyst might enhance the kinetics of hydrogen uptake. The structure of $Mg(AlH_4)_2$ has been recently resolved from X-ray powder diffraction pattern aided by quantum-chemical calculations on cluster models which allowed to tentatively assign also the position of hydrogen atoms, not detectable by X-ray diffraction[8].

In this work, we present an ab-initio study of the thermodynamical and vibrational properties of $Mg(AlH_4)_2$ aiming at providing a better estimate of the decomposition temperature from calculations on periodic models and at confirming the structure inferred experimentally from the comparison of theoretical and experimental IR and Raman spectra.

II. COMPUTATIONAL DETAILS

Calculations are performed within the framework of Density Functional Theory (DFT) with a gradient corrected exchange and correlation energy functional[9], as implemented in the codes PWSCF and PHONONS[10]. Norm conserving pseudopotentials[11] and plane wave expansion of Kohn-Sham (KS) orbitals up to a kinetic cutoff of 40 Ry have been used. Non linear core corrections are included in the pseudopotential of magnesium[12]. Brillouin Zone (BZ) intergration has been performed over Monkhorst-Pack (MP)[13] 6x6x6, 4x4x4 and 16x16x16 meshes for $Mg(AlH_4)_2$, MgH_2 and metallic Al, respectively. Hermite-Gaussian smearing[15] of order one with a linewidth of 0.01 Ry has been used in the reference calculations on metallic Al. Equilibrium geometries have been obtained by optimizing the internal and lattice structural parameters at several volumes and fitting the energy versus volume data with a Murnaghan function[14]. Residual anisotropy in the stress tensor at the optimized lattice parameters at each volume is below 0.6 kbar. Infrared and Raman spectra are obtained from effective charges, dielectric susceptibilities and phonons at the Γ point within density functional perturbation theory[16]. Since $Mg(AlH_4)_2$ is an uniaxial crystal, the infrared absorption spectrum depends on the polarization of the trasmitted electromagnetic wave with respect to the optical axis. Relevant formula for the calculation of the IR and Raman spectra for a polycristalline sample to be compared with experimental data are given in section II.

III. RESULTS

A. Structure and energetics

The structure of $Mg(AlH_4)_2$ has been recently assigned to a CdI_2-like layered crystal from X-ray powder diffraction data[8]. Rietveld refinement assigned the space group $P\bar{3}m1$ (D^3_{3d}) and lattice parameter a=b=5.199 Å and

TABLE I: Experimental and theoretical (in parenthesis) positions (in crystal units) of the four independent atoms at the experimental equilibrium lattice parameters (space group $P\bar{3}m1$, a=5.199 Å, c=5.858 Å). The Wyckoff notation is used. If not reported the theoretical positions coincide with the experimental ones by symmetry. H1 and H2 are non-bridging and bridging hydrogen atoms, respectively.

Mg(1a)	0	0	0
Al(2d)	1/3	2/3	0.7 (0.7053)
H1(2d)	1/3	2/3	0.45 (0.4349)
H2(6i)	0.16 (0.1678)	-0.16 (-0.1678)	0.81 (0.8111)

c=5.858 Å. The position of the four independent atoms in the unit cell are given in Table I. In the AlH_4 tetrahedron there are two Al-H bond lengths: the length of the Al-H1 bond with non-bridging H1 hydrogen aligned with the c axis and the length of Al-H2 bond with the H2 atom bridging between Al and Mg.

A picture of the crystal structure is given in Fig. 1. It can be seen as a stacking along the c axis of AlH_4-Mg-AlH_4 neutral trilayers.

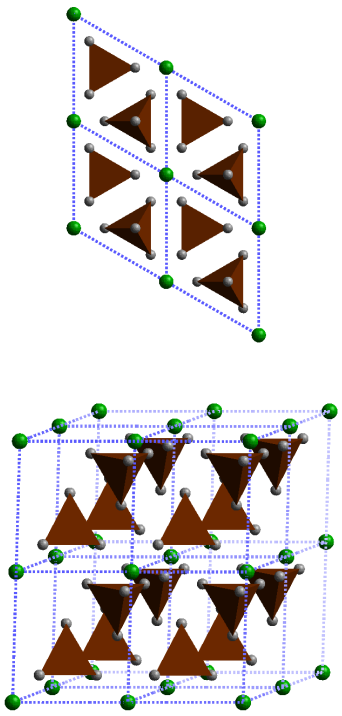

FIG. 1: (Color online) Trigonal structure of $Mg(AlH_4)_2$. The unit cell containing a single formula unit is drawn.

The theoretical equilibrium lattice parameters obtained from the Murnaghan equation of state are a=5.229 Å (exp. 5.199) and c= 6.238 Å (exp. 5.858). In the geometry optimization we have also relaxed the constrained of $P\bar{3}m1$ symmetry, but we have always recovered the experimental space group. The misfit in the c axis (6 %) is larger than usual in DFT-based calculations. As already pointed out in previous cluster calculations on $Mg(AlH_4)_2$[8] the trilayers stacked along the c axis are neutral and not chemically bonded each other. Thus van der Waals interactions have been proposed to play an important role in interlayer cohesion. Since van der Waals interations are not present in current approximations to the exchange and correlation energy functional, the interlayer bonding is underestimated which implies an expansion of the c axis with respect to the experimental data. The energy difference between the relaxed configurations at the experimental and theoretical equilibrium lattice parameters is nevertheless small (38 meV per formula unit). The theoretical atomic positions at the experimental lattice parameters are given in Table I. The theoretical geometry of the AlH_4 tetrahedron is closer to an ideal tetrahedron than the experimental geometry. In fact the theoretical length of the two Al-H bonds are Al-H1= 1.584 Å (exp. 1.46) and Al-H2= 1.614 Å (exp. 1.69). The Al-H bond lengths do not change sizably (within 0.01 Å) by changing the lattice parameters from the experimental values to the theoretical equilibrium values.

The electronic band structure along the high symmetry directions of the Irreducible Brillouin Zone is reported in Fig. 2. The analysis of the projection of the KS states on the atomic orbitals at the Γ point shows that the top of the valence band is mainly formed by 3p states of aluminum and 1s state of hydrogen while the bottom of the conduction band is mainly formed by 3s states of magnesium. The band gap is thus a charge transfer excitation.

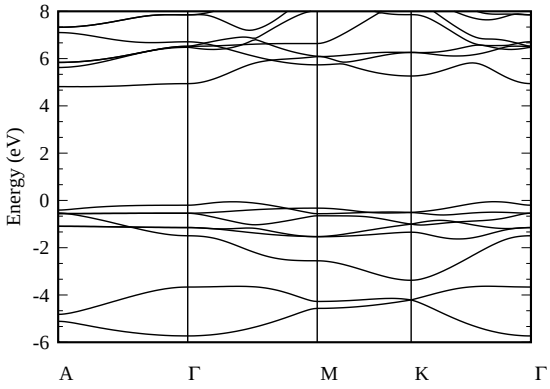

FIG. 2: Electronic band structure along the high symmetry direction of the Brillouin Zone. High symmetry points are labeled following Zak (Ref.[23]). The zero of energy is the top of the valence bands.

By neglecting at first the vibrational contribution to the entropy of the solids, the thermodynamical decomposition temperature T_D of reaction 1 can be estimated

as

$$T_D = \frac{\Delta E + P\Delta V}{3(S_{\mathrm{H_2}} - R)} \tag{2}$$

where ΔV is the difference in volume of the solid reactants and products of reaction 1, P is the pressure, ΔE is the energy difference of reactants and products in 1, $S_{\mathrm{H_2}}$ is the entropy per mole of gaseus H_2 and the gas constant R in the denominator comes from the PV term of gaseus H_2. ΔV and ΔE are obtained from the ab-initio calculations. For MgH_2 the theoretical equilibrium structural parameters are a= 4.470 Å (exp. 4.501[17]), c= 2.943 Å (exp. 3.010[17]) and the $4f$ position (in Wyckoff notation of the $P4_2/mnm$ space group) of the independent H atom in the unit cell is (0.3046,0.3046,0) (exp. (0.3040,0.3040,0)[17]). The theoretical equilibrium lattice parameter of metallic Al is a= 4.065 Å (exp. 4.050 Å[24]). From the total energies at equilibrium we obtain ΔE= 144 kJ/mol (48 kJ/mol per H_2 molecule) which becomes ΔE= 139.5 kJ/mol (46.5 kJ/mol per H_2 molecule) by including the zero point energy of the optical phonons (at the Γ point only) and of the acoustic bands within a Debye model[18]. This result is in good agreement with previous estimate from the extrapolation of cluster calculations (123 kJ/mol[8], 41 kJ/mol per H_2 molecule). The $P\Delta V$ in Eq. 2 is negligible (4.4 J/mol). By assuming $S_{\mathrm{H_2}}$= 130 J/mol K^{-1} at 300 K[19] and atmospheric pressure, we obtain T_D= 111 ^{o}C. The predicted T_D shifts by 2 ^{o}C by including the temperature dependence of $S_{\mathrm{H_2}}$ as given by the Sackur-Tetrode expression[20], the vibrational contribution to the free energy of the solids and the translational and rotational energy of gaseous H_2[18]. The theoretical T_D is comparable with the experimental decomposition temperature which falls in the range 110 ^{o}C - 200 ^{o}C which implies that kinetics effect do not affect dramatically the decomposition reaction of $Mg(AlH_4)_2$.

B. Vibrational properties

Phonons at the Γ-point can be classified according to the irreducible representations of the D_{3d} point group of $Mg(AlH_4)_2$ as Γ= 4 A_{1g} + 2 A_{2g} + 5 E_g + 5 A_{2u} + 6 E_u. A_{1g} and E_g modes are Raman active while A_{2u} and E_u modes are IR active. One A_{2u} and one E_u mode are uniform translational modes. The IR active modes display a dipole moment which couple to the inner macroscopic longitudinal field which shifts the LO phonon frequencies via the non-analytic contribution to the dynamical matrix[16]

$$D^{NA}_{\alpha,\beta}(\kappa,\kappa') = \frac{4\pi}{V_o}\frac{Z_{\alpha,\alpha'}(\kappa)q_{\alpha'}Z_{\beta,\beta'}(\kappa')q_{\beta'}}{\mathbf{q}\cdot\underline{\underline{\varepsilon}}^{\infty}\cdot\mathbf{q}}, \tag{3}$$

where $\underline{\underline{Z}}$ and $\underline{\underline{\varepsilon}}^{\infty}$ are the effective charges and electronic dielectric tensors, V_o is the unit cell volume and $\mathbf{q}$ is the phononic wavevector. The effective charge tensor for the three independent atoms in the unit cell (cfr. Table I) are

$$Z(Mg) = \begin{pmatrix} 2.180 & & \\ & 2.180 & \\ & & 1.974 \end{pmatrix}, \tag{4}$$

$$Z(Al) = \begin{pmatrix} 1.934 & & \\ & 1.934 & \\ & & 1.678 \end{pmatrix}, \tag{5}$$

$$Z(H1) = \begin{pmatrix} -0.627 & & \\ & -0.627 & \\ & & -0.641 \end{pmatrix}, \tag{6}$$

$$Z(H2) = \begin{pmatrix} -0.564 & & \\ & -1.029 & 0.248 \\ & 0.289 & -0.672 \end{pmatrix}, \tag{7}$$

The electronic dielectric tensor is

$$\underline{\underline{\varepsilon}}^{\infty} = \begin{pmatrix} 2.894 & & \\ & 2.894 & \\ & & 2.781 \end{pmatrix}, \tag{8}$$

The calculated phonon frequencies at the Γ point, neglecting the contribution of the longitudinal macroscopic field (Eq. 3), are reported in Table II for the equilibrium geometry at the experimental lattice parameters. The phonon frequencies at the theoretical lattice parameters differ at most by 10 cm^{-1} with respect to those reported in Table II.

For a uniaxial crystal like $Mg(AlH_4)_2$, the macroscopic field contribution to the dynamical matrix (Eq. 3) introduces an angular dispersion of the phonons at the Γ point, i.e. the limit of the phononic bands $\omega(\mathbf{q})$ for $\mathbf{q}\to 0$ depends on the angle θ formed by $\mathbf{q}$ with the optical axis. The angular dispersion of the A_{2u} and E_u modes due to the macroscopic field is reported in Fig. 3.

1. IR spectrum

Tha absorption coefficient of an uniaxial crystal depends on the the polarization of the trasmitted light with respect to the optical axis. The optical properties of the crystal can be obtained from the two dielectric functions $\epsilon_{\perp}(\omega)$ and $\epsilon_{\parallel}(\omega)$ which represent the response of the crystal to electromagnetic wave with electric field perpendicular ($\mathbf{E}\perp\mathbf{c}$) and parallel ($\mathbf{E}\parallel\mathbf{c}$) to the optical axis, respectively. The trasmitted electromagnetic wave at a

TABLE II: Theoretical phonon frequencies at the Γ point, oscillator strengths (f_j in Eq. 10) of IR u-modes and coefficients of the Raman tensor of the Raman active mode, a, b for A_{1g} and c, d for E_g modes (in unit of 10^{-3} V_o= 0.2743 Å^3, see section III B.2). The contribution of the inner longitudinal macroscopic field is not included (LO-TO splitting) (see Fig. 4 for the displacement patterns).

Modes	Energy (cm^{-1})	f_j	a (c)	b (d)
E_g (1)	87		0.976	0.578
A_{2g} (1)	169			
A_{1g} (1)	232		2.337	1.210
E_u (1)	282	3.162		
E_g (2)	298			
A_{2u} (1)	302	0.103		
A_{2g} (2)	355			
E_u (2)	360	0.758		
E_u (3)	620	3.896		
A_{2u} (2)	663	0.784		
E_u (4)	716	0.064		
E_g (3)	742		-0.457	3.653
E_g (4)	758		2.746	0.023
A_{1g} (2)	812		3.970	0.681
A_{1g} (3)	1845		8.768	17.540
A_{2u} (3)	1850	0.072		
E_g (5)	1852		5.202	0.339
E_u (5)	1905	0.597		
A_{2u} (4)	2013	0.040		
A_{1g} (4)	2077		12.270	5.160

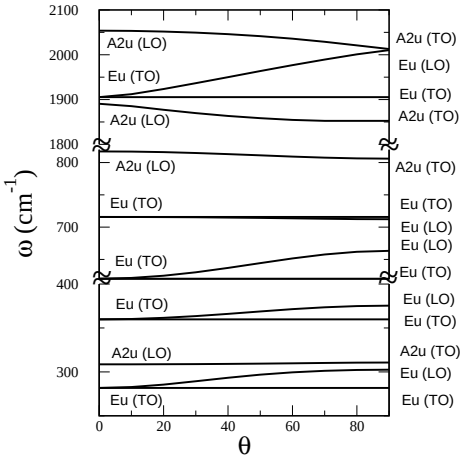

FIG. 3: Angular dispersion of the Γ-point phonons. Only A_{2u} and E_u modes have angular dispersion. θ is the angle formed by the phonon wavevector and the optical axis.

generic wavevector $\mathbf{q}$ forming an angle θ with the optical axis would split in an ordinary wave with electric field perpendicular to the optical axis and in an extraordinary wave with electric field lying in the plane formed by the optical axis and $\mathbf{q}$. The dielectric function $\epsilon_\perp(\omega)$, independent on θ, describes the response to the ordinary waves while the dielectric function $\epsilon_\theta(\omega)$ for the extraordinary wave is θ-dependent and is given by

$$\epsilon_\theta(\omega) = \frac{\epsilon_\perp(\omega)\epsilon_\parallel(\omega)}{\epsilon_\perp(\omega)sin^2\theta + \epsilon_\parallel(\omega)cos^2\theta}. \quad (9)$$

The extraordinary wave coincides with the ordinary wave for $\theta = 0$, i.e. propagation along the optical axis.

$\epsilon_\perp(\omega)$ and $\epsilon_\parallel(\omega)$ can be obtained from ab-initio phonons, effective charges and electronic dielectric tensor as

$$\begin{aligned}\epsilon_\perp(\omega) &= \epsilon_\perp^\infty + \frac{4\pi}{V_o}\sum_{j=1}^{\nu}|\sum_{\kappa=1}^{N}\underline{\underline{Z}}\cdot\frac{\mathbf{e}(j,\kappa)}{\sqrt{M_\kappa}}|^2\frac{1}{\omega_j^2-\omega^2} \\ &= \epsilon_\perp^\infty + \sum_{j=1}^{\nu}\frac{f_j\omega_j^2}{\omega_j^2-\omega^2} \quad (10)\end{aligned}$$

$$\epsilon_\parallel(\omega) = \epsilon_\parallel^\infty + \frac{4\pi}{V_o}\sum_{j=1}^{\mu}|\sum_{\kappa=1}^{N}\underline{\underline{Z}}\cdot\frac{\mathbf{e}(j,\kappa)}{\sqrt{M_\kappa}}|^2\frac{1}{\omega_j^2-\omega^2}, \quad (11)$$

where ν and μ are the number of E_u and A_{2u} TO modes, respectively. The phonons entering in Eq. 10 (11) have wavevector $\mathbf{q}$ parallel (perpendicular) to the optical axis. The notation $\parallel$ and $\perp$ refers to the orientation with respect to the optical axis of the dipole moment of the phonon which coincides with that of the electric field of the trasmitted wave it couples to. The sum over κ run over the N atoms in the unit cell with mass M_κ. $\mathbf{e}(j,\kappa)$ and ω_j are the eigenstates and eigenvalues of the dynamical matrix at the Γ point, without the contribution of the macroscopic field which has no effect on the purely TO modes. The absorption coefficient for the ordinary wave is given by

$$\begin{aligned}\alpha_\perp(\omega) &= \frac{\omega}{nc}\mathrm{Im}\epsilon_\perp(\omega+i\gamma,\gamma\to 0) \\ &= \frac{2\pi^2}{V_o nc}\sum_{j=1}^{\nu}|\sum_{\kappa=1}^{N}\underline{\underline{Z}}\cdot\frac{\mathbf{e}(j,\kappa)}{\sqrt{M_\kappa}}|^2\delta(\omega-\omega_j), \quad (12)\end{aligned}$$

c is the velocity of light in vacuum and n is the refractive index. The absorption coefficient for the extraordinary waves $\alpha_\parallel(\omega)$ with $\mathbf{E}\parallel\mathbf{c}$ (and $\mathbf{q}\perp\mathbf{c}$) is given by the analougous expression by changing ν with μ in the sum over phonons in Eq. 12. The δ-functions in Eq. 12 are approximated by Lorenztian functions as

$$\delta(\omega-\omega_j) = \frac{4}{\pi}\frac{\omega^2\gamma}{(\omega^2-\omega_j^2)^2+4\gamma^2\omega^2}. \quad (13)$$

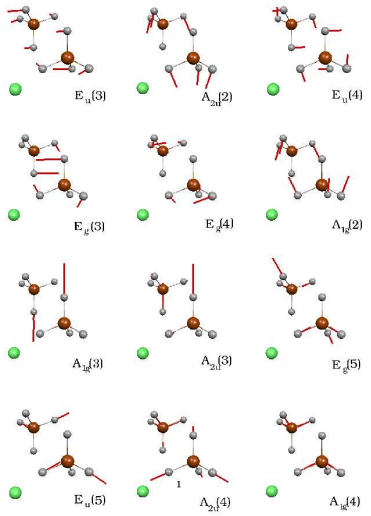

FIG. 4: (Color online) Displacement pattern of the IR and Raman active intra-tetrahedra modes. The lattice modes at lower frequencies are not reported.

The functions $\alpha_\perp(\omega)$ and $\alpha_\parallel(\omega)$ are shown in Fig. 5. The phonons around 700-800 cm^{-1} are bending modes of the Al-H bonds. The highest frequency modes in the range 1800-2000 cm^{-1} are stretching modes of the Al-H bonds. In particular the $A_{2u}(3)$ mode is a stretching of the Al-H_1 apical bond. The other modes are stretching of the Al-H_2 bridging bonds. The displacement pattern of the IR and Raman active modes are shown in Fig. 4. The modes below 360 cm^{-1} (cfr. Table II) are lattice modes involving a rigid motion of the teatrahedra.

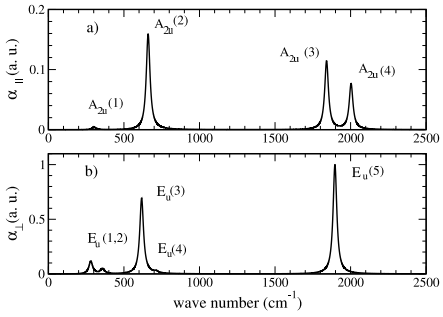

FIG. 5: IR absoption spectrum for a) electric field $\mathbf{E} \parallel \mathbf{c}$ ($\alpha_\parallel$) and for b) $\mathbf{E} \perp \mathbf{c}$ ($\alpha_\perp$). The Lorenztian broadening is γ= 15 cm^{-1} (Eq. 13).

Since the experimental data are available only for a polycrystalline sample[7] an angle-averaged absorption coefficient is needed to compared theoretical and experimental data. For a generic $\mathbf{q}$ forming an angle θ with the optical axis the absorption coefficient for the extraordinary wave can be obtained from the imaginary part of ϵ_θ (Eq. 9). For non-polarized light the total absorption coeffient can be equivalently expressed as

$$\alpha_\theta(\omega) = \frac{2\pi^2}{V_o nc} \sum_{j=1}^{\nu+\mu} |\sum_{\kappa=1}^{N} \hat{\mathbf{q}} \wedge \underline{\underline{Z}} \cdot \frac{\tilde{\mathbf{e}}(j,\kappa)}{\sqrt{M_\kappa}}|^2 \delta(\omega - \tilde{\omega}_j), \quad (14)$$

where $\tilde{\mathbf{e}}(j,\kappa)$ and $\tilde{\omega}_j$ are eigenstates and eigenvalues of the full dynamical matrix including the non-analytic term (Eq. 3) which mixes E_u and A_{2u} modes.

The angle-averaged absorption coefficient has been obtained from Eq. 14 as

$$\alpha_{ave} = \sum_n sin(\theta_n)\alpha_{\theta_n}, \quad (15)$$

where the sum runs over ten angles equally spaced in the range 0-π. The resulting theoretical absorption coefficient for a polycrystalline sample is compared with the experimental IR spectrum in Fig. 6

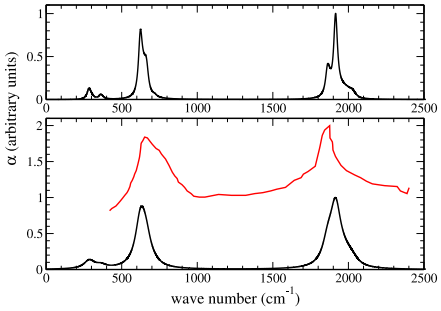

FIG. 6: (Color online) IR absorption spectrum for polycrystalline $Mg(AlH_4)_2$. a) Theoretical spectrum with Lorentzian broadening γ= 15 cm^{-1} (Eq. 13). b) Theoretical spectrum (black line) with γ= 40 cm^{-1} compared with the experimental spectrum (gray line (red online), adapted from Ref.[6]). The experimental spectrum is normalized by setting equal the experimental and theoretical intensity of the highest peak around 1800 cm^{-1}.

Good agreement with experimental data is obtained with a Lorentzian broadening of γ= 40 cm^{-1}. (Fig. 6), but for the experimental shoulder around 800 cm^{-1} which is absent in the theoretical spectra. This misfit might be either due to an underestimation of the $A_{2u}(2)$

mode which is very close to the strongest IR mode $E_{2u}(3)$ (cf. Fig. 5) or to a large inhomogeneous broadening of the experimental spectra. In fact, the line-width of the experimental peak are very large and might be partially due to residual solvent adducts which are released only after dehydrogenation[7].

2. *Raman spectrum*

The differential cross section for Raman scattering (Stokes) in non-resonant conditions is given by the following expression[21,22] (for a unit volume of scattering sample)

$$\frac{d\sigma}{d\Omega d\omega} = \sum_j \frac{\omega_S^4}{c^4} |\mathbf{e_S} \cdot \underline{\underline{R}}^j \cdot \mathbf{e_L}|^2 (n(\omega)+1)\delta(\omega-\omega_j), \quad (16)$$

where $n(\omega)$ is the Bose factor, ω_S is the frequency of the scattered light, $\mathbf{e_S}$ and $\mathbf{e_L}$ are the polarization vectors of the scattered and incident light, respectively. The Raman tensor $\underline{\underline{R}}^j$ associated with the j-th phonon is given by

$$R^j_{\alpha,\beta} = \sqrt{\frac{V_o \hbar}{2\omega_j}} \sum_{\kappa=1}^{N} \frac{\partial \chi^\infty_{\alpha,\beta}}{\partial \mathbf{r}(\kappa)} \cdot \frac{\mathbf{e}(j,\kappa)}{\sqrt{M_\kappa}}, \quad (17)$$

where V_o is the unit cell volume (274.25 Å^3)[8], $\mathbf{r}(\kappa)$ is the position of atom κ-th and $\underline{\underline{\chi}}^\infty = (\underline{\underline{\varepsilon}}^\infty - \delta)/4\pi$ is the electronic susceptibility. The inner longitudinal macroscopic electric field has no effect on g-modes. The tensor $\underline{\underline{R}}^j$ is computed from $\underline{\underline{\chi}}^\infty$ by finite differences, by moving the atoms along the phonon displacement pattern with maximum displacement of 0.002 Å. The Raman tensor (Eq. 16) for the Raman-active irreducible representations has the form

$$A_{1g} \Rightarrow \begin{bmatrix} a & . & . \\ . & a & . \\ . & . & b \end{bmatrix}$$

$$E_g, 1 \Rightarrow \begin{bmatrix} c & . & . \\ . & -c & d \\ . & d & . \end{bmatrix}$$

$$E_g, 2 \Rightarrow \begin{bmatrix} . & -c & -d \\ -c & . & . \\ -d & . & . \end{bmatrix}$$

The coefficients a,b,c and d calculated from first principles as outlined above are given for each mode in Table I.

The experimental Raman spectrum[7] is available only for non-polarized light and backscattering geometry on a polycristalline sample. To compare with experimental data, Eq. 16 must be integrated over the solid angle by summing over all possible polarization vectors $\mathbf{e_S}$ and $\mathbf{e_L}$ consistent with the backscattering geometry. The total cross section for unpolarized light in backscattering geometry is obtained from Eq. 16 with the substitution

$$4\ (\ R^2_{xx}+R^2_{yy}+R^2_{zz}) + 7(R^2_{xy}+R^2_{xz}+R^2_{yz}) + (\ R_{xx}R_{yy}+R_{xx}R_{zz}+R_{zz}R_{yy}) \rightarrow |\mathbf{e_S} \cdot \underline{\underline{R}}^j \cdot \mathbf{e_L}|^2 \quad (18)$$

The resulting theoretical Raman spectrum is compared with experimental data in Fig. 7.

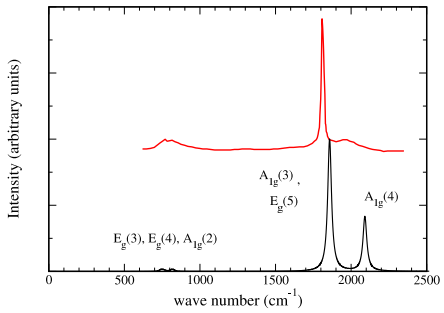

FIG. 7: (Color online) Theoretical (black line) and experimental (gray line (red online), adapted from Ref.[7]) Raman spectra of polycristalline $Mg(AlH_4)_2$ for unpolarized light in backscattering geometry. The experimental spectrum is normalized by setting equal the experimental and theoretical intensity of the highest peak around 1800 cm^{-1}.

The agreement is good, but for the highest frequency peak which is too high in energy and in intensity with respect to experiments. The displacement pattern of the Raman active intra-tetrahedra modes are sketched in Fig. 4. The strongest Raman peak is due to the A_{1g} stretching mode of the Al-H_2 bond at 1845 cm^{-1}.

IV. CONCLUSIONS

Based on Density Functional Theory we have optimized the structure of $Mg(AlH_4)_2$. Due to the lack of van der Waals forces within the current approximations to the energy functional, the interlayer spacing between the neutral AlH_4-Mg-AlH_4 sheets stacked along the c axis is largely overestimated (6 %) in our calculations. Conversely, by fixing the lattice parameters to the experimental ones, the optimization of the internal structure

provides a geometry in fair agreement with that inferred experimentally from x-ray powder diffraction data. The main discrepancy regards the position of the hydrogen atoms (which however can not be detectd accurately from x-ray powder diffraction) resulting in Al-H bond lengths which differ up to 0.1 Å from the exprimental ones. As a consequence, the AlH_4 tetrahedra are much more symmetric in the theoretical geometry than in that proposed experimentally. However, the IR and Raman spectra calculated within density functional perturbation theory are in good agreement with the experimental spectra which supports the correctness of the crystal structure emerged from the ab-initio calculations.

V. AKNOWLEDGMENTS

We gratefully thank G. Benedek, V. Boffa, G. Dai, V. Formaggio and S. Serra for discussion and information. This work is partially supported by the INFM Parallel Computing Initiative.

[1] B. Bogdanović and M. J. Schwickardi, J. Alloys Compd. **253**, 1 (1997).
[2] B. Bogdanović and G. Sandrock, Material Research Bulletin, **27**, 712 (2002).
[3] J. Chen, N. Kuriyama, Q. Xu, H. T. Takeshita, and T. Sakai, J. Phys. Chem. B **105**, 11214 (2001).
[4] H. Morioka, K, Kazizaki, S.-C. Chung, and A. Yamada, J. Alloys Compd. **353**, 310 (2003).
[5] M. Fichtner and O. Furh, J. Alloys Compd. **345**, 286 (2002).
[6] M. Fichtner, O. Furh, and O. Kircher, J. Alloys Compd. **356**, 418 (2003).
[7] M. Fichtner, O. Furh, O. Kircher, and O. Rubner, Mat. Sci. Eng. B **108**, 42 (2004).
[8] M. Fichtner, OJ. Engel, . Furh, A. Glöss , O. Rubner, and R. Ahlrichs, Inor. Chem. **42**, 7060 (2003).
[9] A. D. Becke, Phys. Rev. **A 38**, 3098 (1988); C. Lee, W. Yang, and R. G. Parr, Phys. Rev. **B 37**, 785 (1988).
[10] Pwscf and Phonons, S. Baroni, A. dal Corso, S. de Gironcoli, and P. Giannozzi, http://www.pwscf.org
[11] N. Troullier and J. L. Martins, Phys. Rev. B **43**, 1993 (1991).
[12] S. Louie, S. Froyen and M.L. Cohen, Phys. Rev. B **26**, 1738 (1982).
[13] H. J. Monkhorst, J. D. Pack *Phys. Rev. B* **13**, 5188 (1976).
[14] D. Murnaghan, Proc. Nat. Acad. Sci. USA **30**, 224 (1944).
[15] M. Methfessel and A.T. Paxton, Phys. Rev. B **40**, 3616 (1989).
[16] S. Baroni, S. de Gironcoli, A. Dal Corso and P. Giannozzi, Rev. Mod. Phys. **73**, 515 (2001).
[17] W. H. Zachariasen, C. E. Holley Jr., and J. F. Stamper Jr., Acta Crystallogr. A **16**, 352 (1963).
[18] The zero-point energy per unit cell of the acoustic bands within the Debye model is given by $E_o = 9/8 k_B \Theta_D = (3^7/2^{11}\pi)^{1/3} h\bar{c} V_o^{-1/3}$ (Ref.[24]), where Θ_D is the Debye temperature, V_o the unit cell volume and $\bar{c}$ is the phase velocity of the acoustic branches ($1/3\ v_{LA} + 2/3\ v_{TA}$) averaged over all directions. For Al Θ_D= 394 K. For MgH_2 $\bar{c} \approx 4.5$ km/s, from the phonons calculation in Ref.[25] (by assuming isotropic phase velocities). For $Mg(AlH_4)_2$, $\bar{c} \approx v_Z/3 + v_L 2/3$, where v_Z= 3.75 km/s and v_L= 4.38 km/s are the phase velocities (averaged over the TA and LA branches) along the ΓZ and ΓL directions of the BZ, calculated within dendisty functional pertirbation theory. The zero point energy per unit cell of the optical modes of $Mg(AlH_4)_2$, MgH_2 and H_2 are 162.4, 73.2, and 26.2 kJ/mol, respectively. The contribution of the vibrational modes to the free energy at finite temperature has been computed by considering only the optical phonons at the Γ-point and the acoustic phonons within the Debye approximation as given above.
[19] P.W. Atkins, sl Physical Chemistry, 5th Edition (Oxford University Press, Oxford, 1994), p. C11.
[20] Ref.[19], p. 686.
[21] *Light Scattering in Solids II*, edited by M. Cardona and G. Güntherodt (Springer-Verlag, Berlin, 1982).
[22] P. Brüesch, *Phonons: Theory and Experiments II* (Springer-Verlag, Berlin, 1986).
[23] J. Zak, *Irreducible Representations of Space Groups* (Benjamin, New York, 1969).
[24] N. W. Ashcroft and N. D. Mermin, *Solid State Physics* (Holt-Saunders International Edition, Philadelphia, 1976).
[25] H. G. Schimmel, M. R. Johnson, g. J. Kearey, A. J. Ramirez-Cuesta, J. Huot, and F. M. Mulder, Mat. Sci. Eng. B **108**, 38 (2004).